

Giant formation rates of ultracold molecules via Feshbach Optimized Photoassociation

Philippe Pellegrini, Marko Gacesa, and Robin Côté

Department of Physics, U-3046, University of Connecticut, Storrs, CT, 06269-3046

(Dated: August 23, 2021)

Ultracold molecules offer a broad variety of applications, ranging from metrology to quantum computing. However, forming “real” ultracold molecules, *i.e.* in deeply bound levels, is a very difficult proposition. Here, we show how photoassociation in the vicinity of a Feshbach resonance enhance molecular formation rates by several orders of magnitude. We illustrate this effect in heteronuclear systems, and find giant rate coefficients even in deeply bound levels. We also give a simple analytical expression for the photoassociation rates, and discuss future applications of the Feshbach Optimized Photoassociation, or FOPA, technique.

PACS numbers: 32.80.Pj

In recent years, several techniques, ranging from Stark decelerators to buffer-gas cooling, have been developed to obtain cold molecules [1]. Such molecules are interesting for a range of applications [2] in metrology, high precision molecular spectroscopy, or quantum computing [3]. However, forming ultracold stable molecules in deeply bound levels remains a challenge: most approaches give temperatures still considered *hot* (roughly 100 mK - 1 K). To reach the ultracold regime (below 1 mK), direct laser cooling of molecules is usually not effective due to their rich and complex level structure [4]. Instead, it is possible to create molecules starting from ultracold atoms, via photo-association (PA) or “magneto-association” (MA). While PA occurs when two colliding atoms absorb a photon to form a molecule [2], MA takes advantage of magnetically tuned Feshbach resonances [5].

Over the last decade, PA has been widely used to study long range molecular interactions and to probe ultracold gases [2], and MA to realize molecular condensates [6] and investigate the BEC-BCS cross-over regime [7]. However, both methods usually lead to molecules in highly excited states. According to the Franck-Condon principle, electronic transitions in PA occur at large interatomic distances, leading to molecules in high rovibrational levels that can either decay by spontaneous emission or collisional quenching. To stabilize the molecules in their ground potentials, one could use two-photon schemes [8], or excited molecular states with long-range wells that increase the probability density at short range. This latter solution requires the existence of double-well molecular potentials [4] and cannot be easily generalized. In MA, molecules are produced by sweeping the magnetic field through a Feshbach resonance, which occur when the energy of a colliding pair of atoms matches that of a bound level associated to a closed channel. The molecules produced by MA are in the uppermost states near dissociation [5] and thus relatively extended and fragile.

In this article, we investigate a new PA scheme which uses a magnetically induced Feshbach resonance [5] to enhance the probability density at short range. This Feshbach Optimized Photoassociation (FOPA) allows tran-

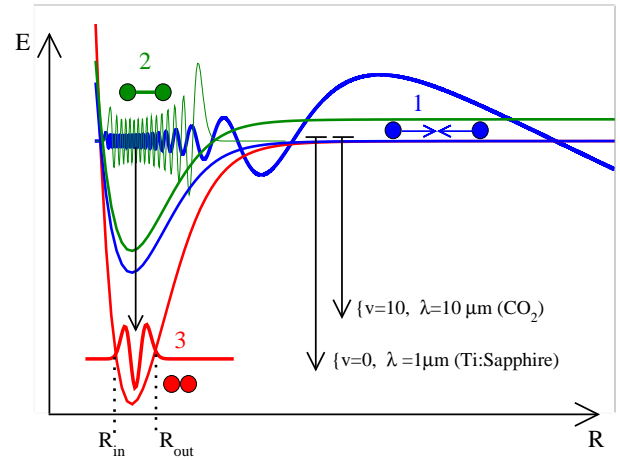


FIG. 1: FOPA: Colliding atoms (1) interact via open (blue) and closed (green) channels due to hyperfine interactions. A Feshbach resonance occurs when a bound level (2) (green wave function) coincides with the continuum state (blue wave function). A photon (wavelength λ) can associate the atoms into a bound level v (3) of the ground state potential (red) with inner and outer classical turning points R_{in} and R_{out} .

sitions even to deeply bound levels (see Fig. 1). Feshbach resonances and PA have been proposed to associate atoms [9] and convert an atomic into a molecular BEC [10]. However, as opposed to previous proposals [11], FOPA takes advantage of the whole wave function in a full quantum coupled-channel calculation, and is thus more general than the Franck-Condon principle.

Feshbach resonances are commonly found in both homonuclear and heteronuclear systems with hyperfine interactions. We focus our attention on heteronuclear systems for which the presence of a permanent dipole moment allows transitions from the continuum directly to a rovibrational level v of the ground electronic molecular states [12] (see Fig. 1). The corresponding photoassociation rate coefficient $K_{PA}^v = \langle v_{rel} \sigma_{PA}^v \rangle$ [2, 8] depends on v_{rel} , the relative velocity of the colliding pair, and on σ_{PA}^v , the PA cross section. The bracket stands for an average over the distribution of v_{rel} , here a Maxwell-Boltzmann

distribution characterized by the temperature T [13]. At low laser intensity I and ultracold temperatures, where only the s -wave contributes significantly, the maximum rate coefficient (neglecting saturation) is [12]

$$K_{\text{PA}}^v = \frac{8\pi^3 I e^{-1/2}}{h^2 c Q_T} |\langle \phi_{v,J=1} | D(R) | \Psi_{\epsilon,l=0} \rangle|^2, \quad (1)$$

where $Q_T = (2\pi\mu k_B T/h^2)^{3/2}$, and $D(R)$ is the appropriate dipole moment for the transition between the initial $|\Psi_{\epsilon,l=0}\rangle$ and final $|\phi_{v,J=1}\rangle$ states corresponding to the s -wave ($l = 0$) continuum wave function of the colliding pair and the populated bound level ($v, J = 1$) wave function. Here k_B , h , and c , are the Boltzman and Planck constants, and the speed of light in vacuum, respectively.

We determine $|\Psi_{\epsilon,l=0}\rangle$ by solving the Hamiltonian for two colliding atoms in a magnetic field [5, 14]:

$$H = \frac{p^2}{2\mu} + V_C + \sum_{j=1}^2 H_j^{\text{int}}. \quad (2)$$

Here, $V_C = V_0(R)P^0 + V_1(R)P^1$ is the Coulomb interaction, decomposed into singlet (V_0) and triplet (V_1) molecular potentials, with the associated projection operator P^0 and P^1 . The internal energy of atom j , $H_j^{\text{int}} = \frac{a_{\text{hf}}^{(j)}}{h^2} \vec{s}_j \cdot \vec{i}_j + (\gamma_e \vec{s}_j - \gamma_n \vec{i}_j) \cdot \vec{B}$, consists of the hyperfine and Zeeman contributions, respectively. Here \vec{s}_j and \vec{i}_j are the electronic and nuclear spin of atom j with hyperfine constant $a_{\text{hf}}^{(j)}$, and \vec{B} is the magnetic field. Since the nuclear gyromagnetic factor γ_n is three orders of magnitude smaller than γ_e , we neglect it in our calculations.

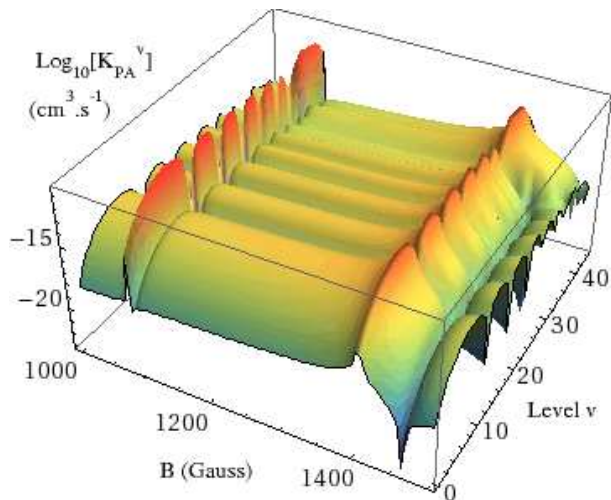


FIG. 2: K_{PA}^v in cm^3/s vs. the B -field ($T = 50 \mu\text{K}$, $I = 1 \text{ W}/\text{cm}^2$) for various levels ($v, J = 1$) of the LiNa $X^1\Sigma^+$ potential, starting from ${}^6\text{Li}(f = \frac{1}{2}, m = -\frac{1}{2})$ and ${}^{23}\text{Na}(f = 1, m = -1)$. Two Feshbach resonances at 1081 and 1403 Gauss enhance the PA rates by several orders of magnitude.

We solve for $|\Psi_{\epsilon,l=0}\rangle$ by using the Mapped Fourier Grid

method [15], and by expanding it onto the basis constructed from the hyperfine states of both atoms,

$$|\Psi_{\epsilon,l=0}\rangle = \sum_{\alpha=1}^N \psi_{\alpha}(R) \{|f_1, m_1\rangle \otimes |f_2, m_2\rangle\}_{\alpha}, \quad (3)$$

where $\vec{f}_j = \vec{i}_j + \vec{s}_j$ is the total spin of atom j , and m_j its projection on the magnetic axis. Here, $\psi_{\alpha}(R)$ stands for the radial wave function associated with channel α labeled by the quantum numbers f_i, m_i ; the Hamiltonian (2) couples channels with the same total projection $M = m_1 + m_2$. As an example, we consider forming LiNa in the ground $X^1\Sigma^+$ electronic state from atoms initially in the ${}^6\text{Li}(f = \frac{1}{2}, m = -\frac{1}{2})$ and ${}^{23}\text{Na}(f = 1, m = -1)$ states ($\alpha = 1$), using the potentials of Ref.[16]. Eight channels with total $M = -\frac{3}{2}$ are coupled, and we found two Feshbach resonances at 1081 and 1403 Gauss. Fig. 2 displays K_{PA}^v as a function of the B -field into different levels ($v, J = 1$) at $T = 50 \mu\text{K}$ and $I = 1 \text{ W}/\text{cm}^2$. Near a resonance, K_{PA}^v is drastically enhanced by up to five orders of magnitude, even for the lowest ($v < 10$) levels. For typical densities ($n_{\text{Li}} = n_{\text{Na}} \sim 10^{12} \text{ cm}^{-3}$) and an illuminated volume V of 1 mm^3 , $N_v = n_{\text{Li}} n_{\text{Na}} V K_{\text{PA}}^v = 2 \times 10^6$ molecules are formed in $v = 0$ at 1403 Gauss (neglecting back-stimulation [8]).

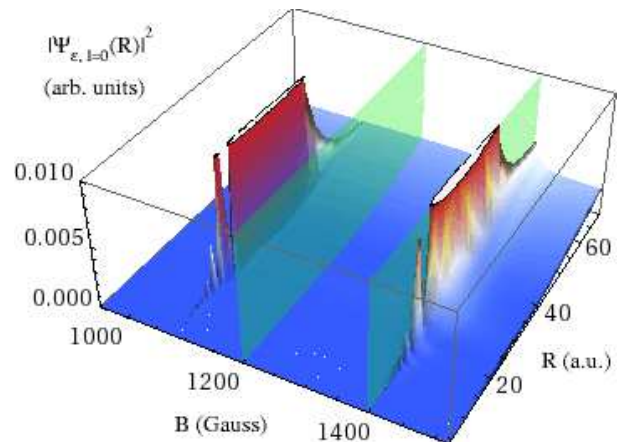


FIG. 3: Probability density $|\Psi_{\epsilon,l=0}(R)|^2$ vs. B . As B nears a resonance, $|\Psi_{\epsilon,l=0}|^2$ increases sharply (truncated above 0.01). Examples of $|\Psi_{\epsilon,l=0}|^2$ off and on resonance (green planes at 1200 and 1400 Gauss, respectively) are shown in Fig. 4.

These giant formation rates can be understood by the sharp increase in the amplitudes of the radial wave functions ψ_{α} in the vicinity of a Feshbach resonance. In Fig. 3, we show the total probability density $|\Psi_{\epsilon,l=0}(R)|^2$ as a function of B . As the magnetic field B nears either of the resonances at 1081 and 1403 Gauss, $|\Psi_{\epsilon,l=0}(R)|^2$ increases by several orders of magnitudes (qualitatively the same for all channels). Fig. 4 shows the total initial probability density $|\Psi_{\epsilon,l=0}(R)|^2$ on and off resonance ($B = 1400$ and 1200 Gauss, respectively): the main effect of the resonance is the appearance of a large peak at

shorter distance near $40 a_0$ (see top panel, inset). This peak is roughly located at the classical outer turning point R_{out} of the bound state associated to the closed channel, usually one of the uppermost bound levels. This is apparent in the top panel, where this peak almost coincides with the outer lobe of $|\phi_{v=44, J=1}(R)|^2$, the uppermost bound level of $X^1\Sigma^+$. We also observe that the off-resonance probability density is very much reduced when compared to on-resonance, leading to a very weak overlap integral in K_{PA}^v . The lower panel shows the short separation range, where the on resonance probability density is much larger than the off resonance case, leading to a substantial overlap integral in K_{PA}^v with deeply bound levels (e.g., $v = 0$ or 4). We also note the more complicated nodal structure of $|\Psi_{\epsilon, l=0}(R)|^2$, a direct result of the hyperfine mixing of the entrance channel $\alpha = 1$ with all other channels ($\alpha = 2, \dots, 8$).

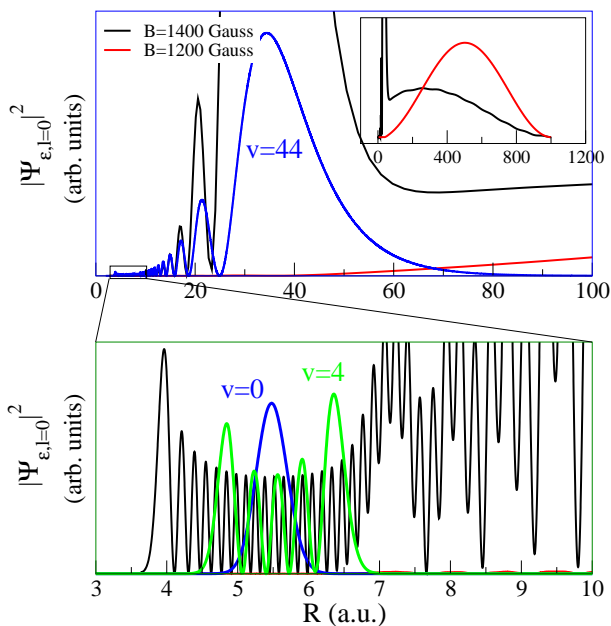


FIG. 4: Probability density on- (black) and off- (red) resonance. The top panel shows that $|\Psi_{\epsilon, l=0}|^2$ gets a peak near $R \sim 40$ a.u. on resonance (inset). The upper bound level $v = 44$ of the singlet ground state is also depicted. The off-resonance density is negligible for $R < 50$ a.u. The bottom panel illustrates the inner region where the more deeply bound target levels v are located (e.g. $v = 0$ and 4). Again, $|\Psi_{\epsilon, l=0}|^2$ is sizable on resonance and negligible off-resonance.

Analytical results are obtained with a two coupled channel model of reduced μ , in which the wave function ψ_1 of the continuum state associated to the open channel 1 (with potential V_1) is coupled to the wave function ψ_2 associated to the closed channel 2 (with V_2) [17]

$$-\frac{\hbar^2}{2\mu} \frac{d^2}{dR^2} \begin{pmatrix} \psi_1 \\ \psi_2 \end{pmatrix} + \begin{pmatrix} V_1 & V_{1,2} \\ V_{2,1} & V_2 \end{pmatrix} \begin{pmatrix} \psi_1 \\ \psi_2 \end{pmatrix} = E \begin{pmatrix} \psi_1 \\ \psi_2 \end{pmatrix}. \quad (4)$$

We assume both coupling terms $V_{1,2}$ and $V_{2,1}$ to be real, and fix the threshold E_1 of channel 1 at $E = 0$. If the

couplings were switched off, the solution for the open channel 1 would be $\psi_1 \rightarrow \psi_{\text{reg}}$ while the closed channel 2 would have a bound state $\psi_2 \rightarrow \psi_0$ with energy E_0 . A resonance occurs when E is near the energy E_0 of ψ_0 . The analytical solutions for Eq.(4) are then [17]

$$\psi_1(R) = \psi_{\text{reg}}(R) + \tan \delta \psi_{\text{irr}}(R),$$

$$\stackrel{R \rightarrow \infty}{=} \frac{1}{\cos \delta} \sqrt{\frac{2\mu}{\pi \hbar^2 k}} \sin(kR + \delta_{\text{bg}} + \delta), \quad (5)$$

$$\psi_2(R) = -\sqrt{\frac{2}{\pi \Gamma}} \sin \delta \psi_0(R). \quad (6)$$

Here δ_{bg} and δ are the background and resonant phase shifts, while $k = \sqrt{2\mu E}/\hbar$. The asymptotic regular and irregular solutions are $\psi_{\text{reg}} = \sqrt{\frac{2\mu}{\pi \hbar^2 k}} \sin(kR + \delta_{\text{bg}})$ and $\psi_{\text{irr}} = \sqrt{\frac{2\mu}{\pi \hbar^2 k}} \cos(kR + \delta_{\text{bg}})$. Finally, the width $\Gamma(E)$ of the resonance may vary slowly with E .

Here, scanning the B -field is equivalent to scanning E , since the position E_0 of the bound state in channel 2 is shifted by the Zeeman interaction. To first order in k , the s -wave phase shifts are related to the scattering length a by $\tan(\delta + \delta_{\text{bg}}) = -ka$, with $\delta_{\text{bg}} = -ka_{\text{bg}}$ and [14]

$$a = a_{\text{bg}} \left(1 - \frac{\Delta}{B - B_0} \right), \quad (7)$$

where a_{bg} is the background scattering length of the pair of atoms (which can slowly vary with B), B_0 is the position of resonance, and Δ is related to $\Gamma(E)$ [14]. Introducing the analytical solutions into Eq.(1) leads to

$$K_{\text{PA}}^v = K_{\text{off}}^v |1 + C_1 \tan \delta + C_2 \sin \delta|^2, \quad (8)$$

where $K_{\text{off}}^v = \frac{8\pi^3}{\hbar^2} \frac{I}{c} \frac{e^{-1/2}}{Q_T} |\langle \psi_v | D | \psi_{\text{reg}} \rangle|^2$ is the off-resonance rate coefficient ($\delta = 0$) with ψ_v the final (target) state, $C_1 = \langle \psi_v | D | \psi_{\text{irr}} \rangle / \langle \psi_v | D | \psi_{\text{reg}} \rangle$ relates to the open channel 1, while the coupling to the bound state ψ_0 in the closed channel 2 is given by $C_2 = -\sqrt{2/\pi \Gamma} \langle \psi_v | D | \psi_0 \rangle / \langle \psi_v | D | \psi_{\text{reg}} \rangle$.

The relative importance of C_1 and C_2 depends on the nodal structure of ψ_v , ψ_{reg} , ψ_{irr} , and ψ_0 . Unless R_{out} of ψ_v accidentally coincides with a node in ψ_{reg} or ψ_{irr} , the overlap integral of ψ_v with both ψ_{reg} and ψ_{irr} are of the same order, leading to $|C_1| \sim 1$. The relative size of C_2 can be controlled by the target level v . For a deeply bound level, R_{out} is at short separation where the overlap with ψ_{reg} is small while the overlap with ψ_0 can be substantial leading to $|C_2| \gg |C_1|$. For very extended levels v , R_{out} of ψ_v is at large separation and the overlap with ψ_0 less important, leading to $|C_2| \ll |C_1|$. Naturally, these behaviours might differ for specific levels v .

The generalization of Eq.(8) to several coupled channels is straightforward as we simply add their contributions. Furthermore, we find that only two or three channels contribute significantly to give these giant formation

rate coefficients. In Fig. 5, we show K_{PA}^v for the ground vibrational level $v = 0$ with the same parameters used in Fig. 2. The top panel depicts the scattering length a with the two Feshbach resonances and its analytical fit. The bottom panel compares the exact numerical results using eight coupled channels with the simple expression (8). In both cases, the agreement is impressive. We verified that similar agreement was obtainable for other levels v , indicating the broad and general validity of Eq.(8).

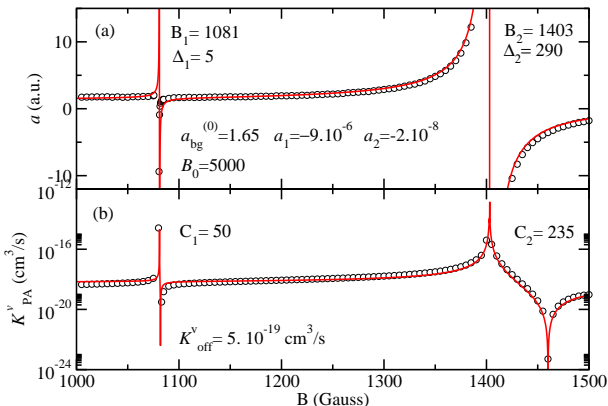


FIG. 5: In (a): scattering length a for full coupled problem (circles) and the fit using $a = a_{\text{bg}}(B)(1 - \frac{\Delta_1}{B-B_1} - \frac{\Delta_2}{B-B_2})$ with $a_{\text{bg}}(B) = a_{\text{bg}}^{(0)} + a_1(B+B_0) + a_2(B+B_0)^2$. In (b): K_{PA}^v for $v = 0$ at $50 \mu\text{K}$ and $1 \text{ W}/\text{cm}^2$ (circles) and the simple formula (8) using $\tan \delta = k a_{\text{bg}}(B)(\frac{\Delta_1}{B-B_1} + \frac{\Delta_2}{B-B_2})$. The numerical parameters are given in each plot [18].

In conclusion, we showed that it is possible to use Feshbach Optimized Photoassociation (FOPA) to form “real” ultracold molecules, *i.e.* in deeply bound levels, in large quantities. In fact, the rate coefficient increases by several orders of magnitude, leading to giant formation rates near Feshbach resonances. We applied this concept to LiNa, an heteronuclear system with a dipole moment. In addition, we gave a simple analytical model describing the FOPA technique. As opposed to other proposals using the Franck-Condon principle for transition near the turning point R_{out} of the closed channel, FOPA takes advantage of the full wave function and its amplification in the vicinity of a Feshbach resonance, making it a general technique. In fact, FOPA could be used to do the spectroscopy of more deeply bound levels of excited electronic states which are usually not reachable by standard PA, bridging the gap between traditional spectroscopy for deep levels and PA of high-lying levels realized with ultracold atoms. Also, by targeting levels v for which C_1 or C_2 is dominant, it is possible to determine the parameters of the scattering length (a_{bg} , Δ , and B_0) by pure spectroscopic measurements. This offers an accurate non-destructive method to first detect a Feshbach reso-

nance, and then obtain the scattering length parameters. Finally, we note that this enhancement will be present in other manifestation of Feshbach resonances, such as those obtained via electric fields [19] or magnetic dipolar interactions (*e.g.*, in Cr [20]). This is a very general technique which can be applied to bosonic, fermionic or mixed species, where Feshbach resonances exist.

This research was supported by the U.S. Department of Energy, Office of Basic Energy Sciences.

-
- [1] J. Doyle *et al.*, Eur. Phys. J. D **31**, 149 (2004), and references therein.
 - [2] K.M. Jones, E. Tiesinga, P.D. Lett, and P.S. Julienne Rev. Mod. Phys. **78**, 483 (2006).
 - [3] D. DeMille, Phys. Rev. Lett. **88**, 067901, (2002); S.F. Yelin, K. Kirby, and R. Côté, Phys. Rev. A **74**, 050301(R) (2006).
 - [4] A. Fioretti *et al.* Phys. Rev. Lett. **80**, 4402 (1998); M. D. Di Rosa, Eur. Phys. J D **31**, 395 (2004).
 - [5] T. Köhler, K. Góral, and P.S. Julienne, Rev. Mod. Phys. **78**, 1311 (2006).
 - [6] S. Jochim *et al.*, Science **302**, 2101 (2003); M. Greiner, C.A. Regal, and D.S. Jin, Nature **426**, 537 (2003); M.W. Zwierlein *et al.*, Phys. Rev. Lett. **91**, 250401 (2003).
 - [7] D. E. Miller *et al.*, Phys. Rev. Lett. **99**, 070402 (2007); A. Altmeyer *et al.*, Phys. Rev. Lett. **98**, 040401 (2007); G.B. Partridge *et al.*, Phys. Rev. Lett. **95**, 020404 (2005); M. Greiner, C.A. Regal and D.S. Jin, Phys. Rev. Lett. **94**, 070403 (2005).
 - [8] E. Juarros, R. Côté, and K. Kirby, Eur. Phys. J. D. **31**, 213 (2004); E. Juarros, K. Kirby, and R. Côté, J. Phys. B **39**, S965 (2006).
 - [9] F.A. van Abeelen *et al.*, Phys. Rev. Lett. **83**, 1550 (1999).
 - [10] S. J. J. M. F. Kokkelmans, H. M. J. Vissers, and B. J. Verhaar Phys. Rev. A **63**, 031601 (2001) T. Hornung, S. Gordienko, R. de Vivie-Riedle, and B. J. Verhaar Phys. Rev. A **66**, 043607 (2002)
 - [11] B. Laburthe *et al.*, Europhys.Lett. **64**, 171 (2003); W.C. Stwalley, Eur. Phys. J D **31**, 221 (2004); F.A. van Abeelen, D.J. Heinzen, and B.J. Verhaar, Phys. Rev. A **57**, R4102 (1998).
 - [12] E. Juarros, P. Pellegrini, K. Kirby, and R. Côté, Phys. Rev. A, **73**, 041403(R) (2006).
 - [13] This T -dependence is valid at all T for mixed species.
 - [14] A.J. Moerdijk, B.J. Verhaar, and A. Axelsson, Phys. Rev. A, **51**, 4852 (1995).
 - [15] V. Kokouline, O. Dulieu, R. Kosloff, and F. Masnou-Seeuws J. Chem. Phys. **110**, 9865 (1999)
 - [16] M. Gacesa, P. Pellegrini, R. Côté, arXiv:0709.2924.
 - [17] Harald Friedrich Theoretical Atomic Physics, Springer-Verlag Berlin Heidelberg 1990
 - [18] C_1 and C_2 and are supposed B independent.
 - [19] Z. Li and R.V. Krems, Phys. Rev. A **75**, 032709 (2007).
 - [20] J. Werner *et al.*, Phys. Rev. Lett. **94**, 183201 (2005); Z. Pavlovic, R.V. Krems, R. Côté, and H.R. Sadeghpour, Phys. Rev. A **71**, 061402(R) (2005).